NANO LETTERS

2007
Vol. 7, No. 11
3329−3335

Direct Observation of Brownian Dynamics of Hard Colloidal Nanorods

Hideatsu Maeda*,† and Yoshiko Maeda‡

National Institute of Advanced Industrial Science and Technology (AIST), Institute for Biological Resources and Functions, AIST Tsukuba Central 6, 1-1-1 Higashi, Tsukuba, Ibaraki, 305-8566 Japan, and The University of Tsukuba, 1-1-1 Tennodai, Ibaraki 305-8574, Japan

Received July 2, 2007; Revised Manuscript Received August 27, 2007

ABSTRACT

We synthesize monodisperse selenium (Se) colloidal rods, and the suspensions exhibit the smectic phase at a particle volume fraction (ϕ) of 0.28. Side-by-side rod clustering occurs at $\phi > 0.04$. Cluster-size distributions and persistence times are determined for various ϕ. In dense suspensions ($\phi > 0.1$), individual rods reveal characteristic fundamental motions, e.g., reptation and synchronized rotation. Mean-square displacements of the rods suggest a cage trapping and escape. Estimated translational and rotational diffusion coefficients show a large difference from predictions by computer simulations.

Rodlike colloids can form a variety of positional and orientational ordered structures depending on ϕ. Onsager theoretically showed that hard thin rods can form nematic structures purely by an excluded volume effect.[1] By using computer simulations, phase diagrams for hard spherocylinders (HSC) have been determined as a function of the aspect ratio and ϕ of the HSCs, demonstrating that more different types of ordered phases can be formed by the excluded volume effect.[2,3] Moreover, phase diagrams for attractive[4] and repulsive[5] HSCs have been calculated. Experimentally, various types of rods, such as inorganic colloids,[6−10] latex,[11] and (TMV[12] and fd[13,14]) viruses, have been found to form various liquid crystalline structures and besides phase diagrams have been determined for some colloidal rod systems.[9,10,13,14]

Accordingly, it is of great interest and significance to study the dynamical behavior of rods in solutions (suspensions). For long thin rods, the entanglement effect between neighbors restricting their rotations and lateral translations becomes remarkable in semidilute solutions. This is the so-called "reptation motion", and to theoretically explain such rod dynamics, the "tube model" was introduced by Doi and Edwards.[15,16] Using computer simulations, Frenkel and Maguire first investigated density-dependent dynamics for long thin rods in the isotropic phase,[17] and subsequently, aspect-ratio- and density-dependent translational and rotational diffusivities of hard rods in the isotropic and/or nematic phases have been studied.[18−22] Moreover, Brownian dynamics simulations of repulsive rods[23] and of hard core rods in fixed discs[24] have been carried out.

Experimentally, using various bulk techniques, e.g., dynamic light scattering,[25] electric birefringence,[26] and fluorescence recovery after photobleaching (FRAP),[27,28] translational (D_T) and/or rotational (D_θ) diffusion coefficients of colloidal rods in isotropic suspensions have been measured. In addition, the anisotropy of D_T of rods in the nematic phase has been studied using FRAP[29] or fluorescence microscopic techniques.[30]

However, microscopic dynamics of individual rods cannot be shown by traditional bulk methods involving a large ensemble of rods. With monodisperse colloidal rod suspensions, we previously found side-by-side clustering of the rods and subsequent stacking of the clusters for the formation of smectic domains.[9,10] In this work, by direct observation of the dynamics of individual Se rods in suspensions, we find some fundamental motion modes of the rods and determine the persistence times of the clusters together with the cluster size distributions. We also measure mean-square translational and rotational displacements of the rods and discuss the association of their characteristics with the observed microscopic dynamics of the rods.

Two-Dimensional Brownian Motions. Monodisperse Se rod-ike colloidal particles of $L = 820 \pm 69$ nm (length), $W = 230 \pm 25$ nm (width) (but these were misprinted in ref 9), and $L/W = 3.5$ were synthesized by adding hydrazine solutions of metallic selenium to water.

For imaging, an inverted metallurgical optical microscope equipped with a 100× oil immersion objective lens were used (Figure 1). We left Se rod suspensions in a glass cell

* Corresponding author.
† National Institute of Advanced Industrial Science and Technology.
‡ The University of Tsukuba.

10.1021/nl071577i CCC: $37.00
Published on Web 10/03/2007

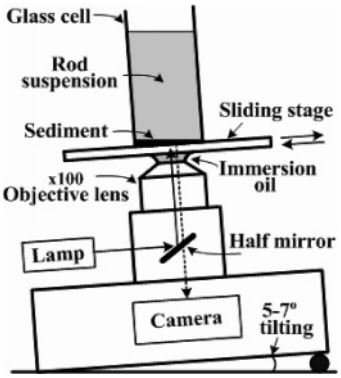

Figure 1. Schematic diagram of our observation system using an inverted metallurgical optical microscope. The entire system is tilted by 5−7° to produce the density gradient in the sediment of Se rods along the cell bottom plane with which the density-dependent Brownian dynamics of the rods can be observed by sliding the sample stage of the microscope.

tilting at an angle of 5−7° until they reached equilibrium and obtained concentration-gradient sediments of the rods on the cell bottom. The tilting cell enabled us to observe concentration-dependent dynamical behavior of the rods all together from the side of the cell bottom. In dense regions of the sediments, the rods exhibit two-dimensional (2D) or quasi-2D Brownian motions in a thin layer on the cell bottom. With decreasing sediment density, the number of rods coming in and out of the thin layer gradually increases, and the rods finally exhibit 3D-Brownian motion over the cell bottom. To find the time-dependent positional and angular displacements of the Se rods near the cell bottom surface, the central point (center-of-mass) and central line of the target rods in each of the sequential assembly images taken by video microscopy are determined by using image analysis software. Currently, single particle tracking techniques are being widely used to determine the movement of, e.g., individual membrane proteins or lipids (labeled with fluorescent particles) at the cell surface with nm spatial resolution.[31]

Volume Fractions of Rods. Although it is not easy to directly measure the rod densities in a thin layer just above the cell bottom, they can be determined by utilizing the following experimental information: (1) the number of rods in the thin layer, (2) 2D images of the rods projected on the cell bottom plane, and (3) the brightness of the individual rods, depending on the vertical distance from the cell bottom. In this work, however, we use a more convenient method as follows. The rods in the thin layer are divided into two types: ones orienting almost parallel to the cell bottom plane, which undergo 2D Brownian motions, and ones coming in and out of the thin layer. The mean numbers of the former and latter rods are denoted by N_r and N_f, respectively. The rod volume fraction, ϕ, in the thin layer with a volume of V is $(v_r N_r + \langle v_f \rangle N_f)/V$, where v_r is the full volume of one rod, v_f the volume of the entering part of one coming-in and -out rod in the thin layer, and $\langle v_f \rangle$ is an averaged value of v_f. The number N_r is very small at low densities, and N_f is almost 0 in the Sm phase. The partial volume v_r is a function of the orientational angle and end position of the rod with respect to the cell bottom plane, which is easily formulated geometrically. The thickness of the thin layer, H_0, is expected to be slightly larger than the focal depth of the optical microscope used because slightly out-of-focus rods that are still interacting with neighbors in the thin layer are also included. By using several experimental facts that (i) no rods stacked right on the bottom rods are visible and (ii) the rod width (W) and the face-to-face separation between rods are 230 nm and typically 200 nm, respectively, we estimate H_0 to be about 430 nm. For comparison of our experiments with 2D Brownian dynamics simulations, the surface density (coverage) of the rods, ρ, is used instead of ϕ, which is approximated by $(H_0/W)\,\phi$. (This equation is almost correct for the smectic phase where most of the rods orient parallel to the cell bottom.)

Images of Rod Arrangement and Cluster Length Distribution. Figure 2 shows optical microscopic images of Se rod suspensions of $\phi = 0.26$, 0.18, 0.042. For $\phi = 0.26$ (Figure 2a), stringlike clusters with various lengths are compactly packed; the clusters are formed from rods aligning side-by-side, and the term "cluster size (length)" indicates the number of rods forming each cluster. The longest cluster in Figure 2a consists of 17 particles (abbreviated 17PC or 17particles-cluster). In small dark regions of this image, only the end of the rods is seen, oriented perpendicular to the image plane. For $\phi = 0.18$ (Figure 2b), the cluster length becomes shorter and the dark regions become larger. For $\phi = 0.042$ (Figure 2c), 2−4PCs are observed, but their contact times are very short (see the section Persistence Time of Clusters). The interparticle distance becomes larger, and the positions and orientational angles of the rods with respect to the cell bottom vary.

Figure 3 shows the relationship between the cluster length and its occurrence in an image area of 550 μm^2 for $\phi = 0.11-0.28$. As ϕ increases, the number of shorter clusters decreases, while that of longer ones increases. In the log−log representation, the curves decrease almost linearly with increasing cluster length, whose slopes are −3.47 for $\phi = 0.11$, −2.74 for $\phi = 0.18$, −2.13 for $\phi = 0.21$, −1.54 for $\phi = 0.26$, and −1.32 for $\phi = 0.28$ (the smectic phase) (indicating that the distribution functions of cluster length, n, can be approximated by the form of n^k, where k corresponds to the slopes), followed by a more drastic reduction at a cluster length of 4 for $\phi = 0.11$, 9 for $\phi = 0.18$, 11 for $\phi = 0.21$, 14 for $\phi = 0.26$, and 20 for $\phi = 0.28$. Such drastic reductions may be characteristic of repulsive rods. In fact, we have found that the smectic phase for attractive β-FeOOH rods exhibits a monochrome interference color over a wide region in dense suspensions, while that for repulsive ones consists of many mosaic-like smectic domains exhibiting different interference colors.[9,10] Thus, a cutoff cluster length (depending on ϕ) may exist for repulsive rod systems. The inset of Figure 3 shows ϕ dependence of the mean cluster length (MCL); it begins to markedly increase at around $\phi = 0.2$ and reaches 6.8 at $\phi = 0.28$ (the smectic phase).

Fundamental Microscopic Motions of Se Rods. By microscopic observation, we find the following fundamental

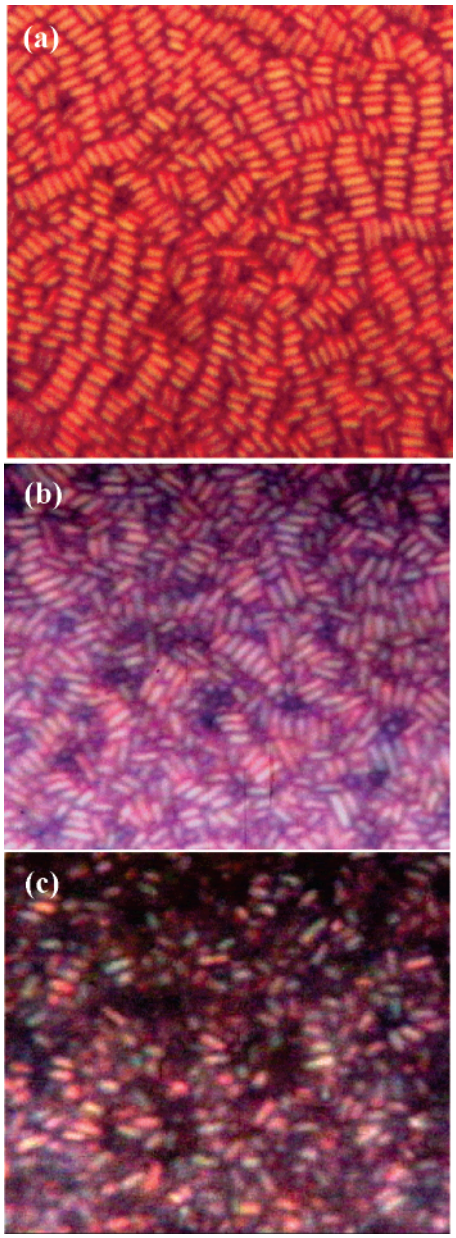

Figure 2. Optical microscopic images of Se rod suspensions of (a) $\phi = 0.26$, (b) 0.18, and (c) 0.042.

moving modes for repulsive Se rods as shown in Figure 4a−f, which are illustrations copied from real motion images taken for $\phi = 0.11$ and 0.18 suspensions (e.g., like Figure 2b), where the rod width is modified to be thinner than the real one.

a. Synchronized Rotational Motions. Rotational Brownian motions of cluster rods are synchronized. For $\phi = 0.18$, the rods of 3−4PCs can have rotational amplitudes (displacements) of 0−40° depending on the structures and dynamics of their neighbors. The mean angular velocity, e.g., for an angular amplitude of 35°, is approximately 0.1°/ms. Figure 4a is a series of snapshots of a synchronized rotation of 4PC rods for $\phi = 0.18$ at elapsed times of 0 (blue), 0.38 (green), and 0.67 s (black), where the four rods all rotate together to have a rotational displacement of about 35° after 0.67 s. For $\phi = 0.11$, cluster rods can have similar rotational amplitudes

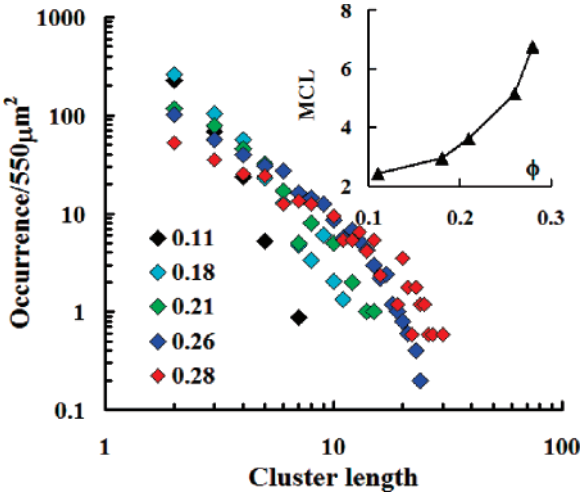

Figure 3. Relationship between Se rod cluster length and occurrence per 550 μm^2 and ϕ dependence of mean cluster length, MCL (inset).

to those for $\phi = 0.18$, but the angular velocities are, e.g., 0.1−0.4°/ms for an angular amplitude of 35°.

b. Translational Motions. We find that, when two rods meet, they tend to align side-by-side to undergo translational and rotational Brownian motions even though they interact repulsively. Figure 4b is a series of snapshots of a rod motion of a 2PC in $\phi = 0.11$ at elapsed times of 0 (blue), 2.7 (green), and 4.0 (black) s, where the rods together undergo a translational motion while rotating and the translational displacement depends on the structures and dynamics of their neighbors. On the other hand, for $\phi = 0.11$ and 0.18, 2PCs exhibiting rotations with very large amplitudes but no translational displacements are often observed. Like discs, this is because the aspect ratios of the 2PCs are close to 1. The translational displacement of the whole cluster drastically decreases with increasing cluster length; for clusters with length ≥4, the rods predominantly show translational fluctuations within the clusters, although still undergoing synchronized rotation.

c. Combination of Clusters. Clusters increase their length by combining with neighboring rods or clusters. The formation of 2PCs is the simplest case. The formation and sustention of 2PCs are essential for cluster growth, and thus 2PCs may be nuclei for clustering of repulsive rods. Even at $\phi = 0.015$, 2PCs are formed, but their contact time is less than 0.04 s. Figure 4c is a series of snapshots of a 6PC formation process for $\phi = 0.18$ at elapsed times of 0 (blue), 0.17 (green), and 0.38 (black) s, where the right-side 3PC rotates by 36° (the curved blue arrow) to join with the left-side neighboring 3PC after 0.38 s.

d. Splitting of Clusters. By repeated creation, combination, and splitting, clusters continuously change their length, orientation, and position. Splitting of clusters is caused by collisions with neighboring rods or clusters and by the escape of rods from the clusters. Figure 4d is a series of snapshots of the cluster splitting process at elapsed times of 0 (blue), 0.50 (green), and 0.83 (black) s for $\phi = 0.18$, where (from the upper side) a rod with an arrowhead (green) partially comes into the 8PC (upper cluster) after 0.50 s and from

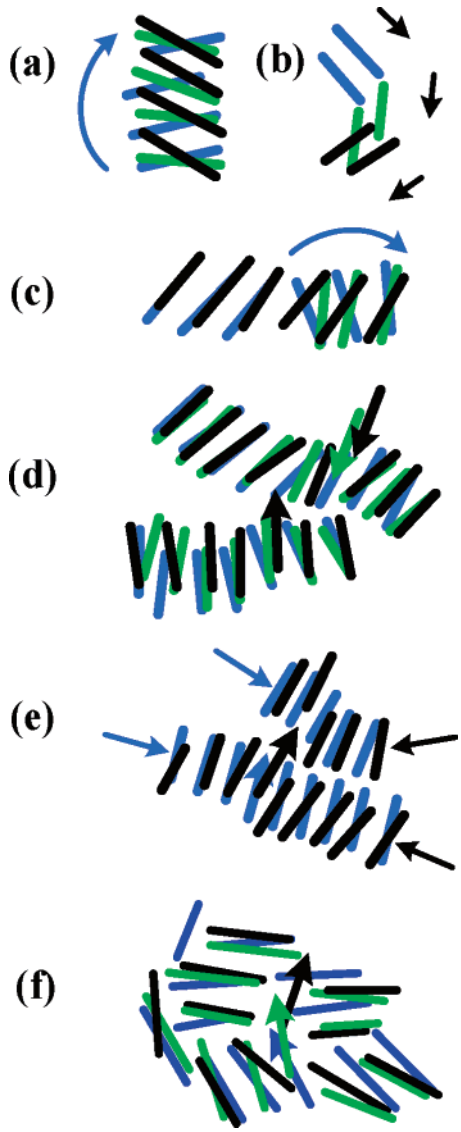

Figure 4. Series of snapshots of fundamental motions of Se rods in suspensions, where the time lapses in the order blue, green, and black: (a) synchronized rotational motion, (b) synchronized translational motion, (c) joining of two clusters, (d) splitting of clusters, (e) branching of clusters, (f) reptation-like motion of a single rod (with an arrowhead).

beside (from below) a rod with an arrowhead (lower black) escaping from the 7PC (lower cluster) partially enters into the 8PC after 0.83 s to split it.

e. Branching of Clusters. Figure 4e is a series of snapshots of the cluster branching process for $\phi = 0.18$ at elapsed times of 0 (blue) and 0.46 (black) s, where, from a 9PC (lower, blue) and 5PC (upper, blue), each pointed out by the thin blue arrow, one 2PC (upper, black) and one cluster with two branches (each pointed out by the thin black arrow) are created. As clearly seen, from the 9PC, a black rod with an arrowhead partially enters by half into the next 5PC after 0.46 s to form a branching structure. However, rods in clusters can also enter perfectly into neighboring parallel-aligned clusters, and such motion of the rods is the elementary step for the longitudinal translational diffusion of rods in the Sm phase.

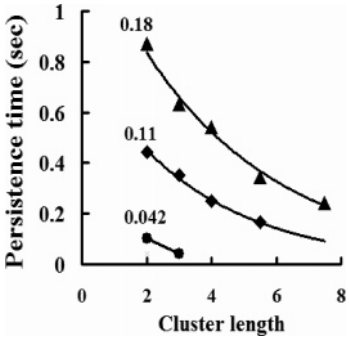

Figure 5. Persistence times against cluster length of 2−8 of Se rods for $\phi = 0.042$, 0.11, and 0.18.

f. Reptation-like Motions of Escaping Rods. When open spaces are formed in the vicinity of clusters, rods can escape there from the clusters. Figure 4f is a series of snapshots of the reptation process of an escape rod (with an arrowhead orienting its moving direction) for $\phi = 0.18$ at elapsed times of 0 (blue), 0.39 (green), and 0.54 (black) s, where as the escape rod moves, the neighbors change their position and orientation. In suspensions of $\phi = 0.18$, lateral translational motions are drastically restricted but sometimes observed only in low-density regions (temporarily formed). For $\phi = 0.11$, the reptation distance (tube length) becomes longer than that for $\phi = 0.18$, and reptation rods additionally exhibit fast-rotational and lateral-translational fluctuations with small amplitudes resulting from an increase of inter-rod separations. For $\phi = 0.042$, the reptation-like motions are observed only in high-density regions (temporally appearing), while such motions are not observed for $\phi = 0.015$.

Persistence Time of Clusters. A tracking observation of individual rods reveals that, after each rod joins (forms) clusters with various lengths during a certain time, depending on ϕ, it becomes single. On the other hand, the length of clusters is constantly changed by collision and combination, and thus we measure ϕ dependence of a time during which each cluster persists in its length, defined here as persistence time (PT). For $\phi = 0.015$, clusters are mostly 2PCs, whose PTs are less than 0.04 s, and the PTs for 3−4PCs are still shorter. Figure 5 shows the PTs of 2−8PCs for $\phi = 0.042$, 0.11, and 0.18. In each ϕ, the PT decreases as the cluster length increases; this is because longer clusters have a higher frequency of collision with neighbors than shorter ones. However, for each cluster length, the PT increases with increasing ϕ; this is because the increase of ϕ reduces the free space near the clusters to suppress their deformation or splitting due to the collision. As shown in Figure 5, when ϕ increases by 4 times, the PTs increase by approximately 10 times. This can also cause a nonlinear increase of the mean cluster length with ϕ as in the inset of Figure 3.

Mean-Square Translational Displacements. Figure 6a shows mean-square translational displacements of the center-of-mass, $\langle R(t)^2 \rangle$, of Se rods in suspensions of $\phi = 0.015$−0.18 and of the rods in free 4−10PCs (F-PC) and constrained 4−8PCs (C-PC) formed in suspensions of $\phi = 0.18$. "Free clusters" means clusters that can naturally change their length with time, and "constrained clusters" means clusters that are constrained between two separated rods tightly adsorbed on

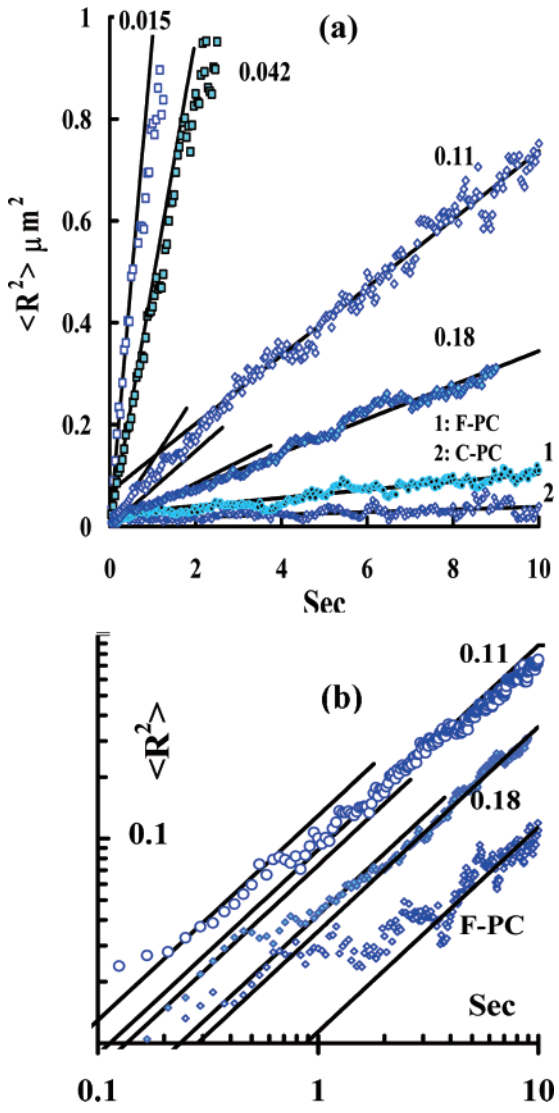

Figure 6. (a) Mean-square translational displacements of the center-of-mass, $\langle R(t)^2\rangle$, of Se rods for $\phi = 0.015-0.18$, and for the free 4−10 PCs (F-PC) and constrained 4−8 PCs (C-PC) in $\phi = 0.18$, where two straight lines of each curve show its initial and final slopes, respectively. (b) Log−log representation of $\langle R(t)^2\rangle$ for $\phi = 0.11$, 0.18, and for the free 4−10 PCs (F-PC). The respective straight lines have unit slope, and the number of each curve denotes ϕ.

the cell bottom surface and thus do not change their length although exhibiting synchronized rotational and in-cluster translational fluctuations. (The average is taken against approximately 100 rods.) For $\phi = 0.015$ and 0.042, $\langle R(t)^2\rangle$ slightly deviates from the initial slope at 1−2 s but exhibits a significant deflection at around 0.5 s for $\phi \geq 0.11$. With increasing ϕ, the deflection is intensified. For the constrained 4−8PCs, $\langle R(t)^2\rangle$ is almost flat above 0.67 s, and such a shape of the curve generally suggests that the particles are confined in a cage to undergo Brownian motions.[31] The rod motions for the constrained 4−8PCs start from a cluster state, and thus the cage effect must be induced by the rod confinement to the clusters.

The feature of $\langle R(t)^2\rangle$ for the dense suspensions can be more clearly presented by the log−log representation as in Figure 6b, where a shoulder or plateau is seen between two lines of unit slope (i.e., $\langle R(t)^2\rangle \propto t$) for $\phi = 0.11$, 0.18, and the free 4−10PCs, showing that $\langle R(t)^2\rangle$ has three regimes of short- and long-time diffusive motions and a plateau between them. For the free 4−10PCs, the shoulder (plateau) appears at 0.6−3.5 s, which must also be due to the confinement of rods to the clusters because the motions of the rods start at a cluster state as well as for the confined 4−8PCs. (An upturn of unit slope after the plateau is also observed in $\langle R(t)^2\rangle$ for dense colloidal sphere systems[32] and explained as due to normal linear diffusion of spheres which escape from a cage.[33]) As in Figure 6a, the long-time diffusion regime begins at around 1.5 s for $\phi = 0.11$, 2.5 s for $\phi = 0.18$, and 3.5 s for the free 4−10PCs; this time delay can be explained as follows: (i) the increase of ϕ makes the PTs longer (Figure 5), and (ii) the increase of ϕ induces the formation of longer clusters (Figure 3) and the rods in the clusters can reside in more different clusters until they become single.

In brief, it is suggested that: (i) the plateau is caused by the confinement of rods to clusters, and (ii) the short- and long-time translational diffusions are due to in-cluster rods and escape rods (from clusters), respectively.

Mean-Square Rotational Displacements. Figure 7a shows mean-square rotational displacements, $\langle\theta(t)^2\rangle$, of the Se rods for $\phi = 0.015-0.18$ suspensions and the free 4−10CPs (F-PC) in $\phi = 0.18$; $\langle\theta(t)^2\rangle$ slightly deviates from an initial straight line around 0.6 s for $\phi = 0.042$, while it significantly deflects near 1.5−2 s for $\phi \geq 0.11$. Figure 7b shows $\langle\theta(t)^2\rangle$ of Se rods for $\phi = 0.11$ and 0.18 in the log−log representation, where a shoulder or plateau appears between two straight lines of unit slope (1.5−4.5 s), implying a caging behavior and two different rotational diffusive motions. As described above, $\langle R(t)^2\rangle$ suggests that the short- and long-time translational diffusive motions are associated with cluster rods and escape rods, respectively; consequently, for $\langle\theta(t)^2\rangle$, the short-time rotational diffusion may be due to synchronized rotations of the cluster rods, while the long-time one may be ascribed to reptation-rotation of the escape rods. Such deflections have also been observed in $\langle R^2\rangle$ and $\langle\theta^2\rangle$ curves calculated by computer simulations for a rod system.[24]

Translational Diffusion Coefficients. The two-dimensional translational (2D) diffusion coefficient, D_T, is obtained using the equation, $D_T = \langle R(t)^2\rangle/4t$. In fact, Table 1 shows the short- and long-time diffusion coefficients, D_T^s and D_T^l, respectively, estimated for Se rods in $\phi = 0.015-0.18$, and for the free 4−10PCs (F-PC) in $\phi = 0.18$. On the other hand, the 2D translational diffusion coefficient of noninteracting rods, D_T, is obtained by using the formulations of Tirado et al.,[34]

$$D_T^0 = k_B T\,(3 \ln P + 0.425 + 2.145/P - 0.033/P^2)/8\pi\eta L \qquad (1)$$

where k_B is the Boltzmann constant, T the absolute temperature, P the rod aspect ratio, and η the solvent viscosity. By substituting the dimensions of the Se rod ($L = 0.82$ μm, $W = 0.23$ μm), $P = L/W = 3.5$, $T = 300$ K, and $k_BT/\eta = 4.14$ μm^3/s into eq 1, D_T^0 is obtained as 0.987 μm^2/s. Using this value, normalized translational diffusion coefficients,

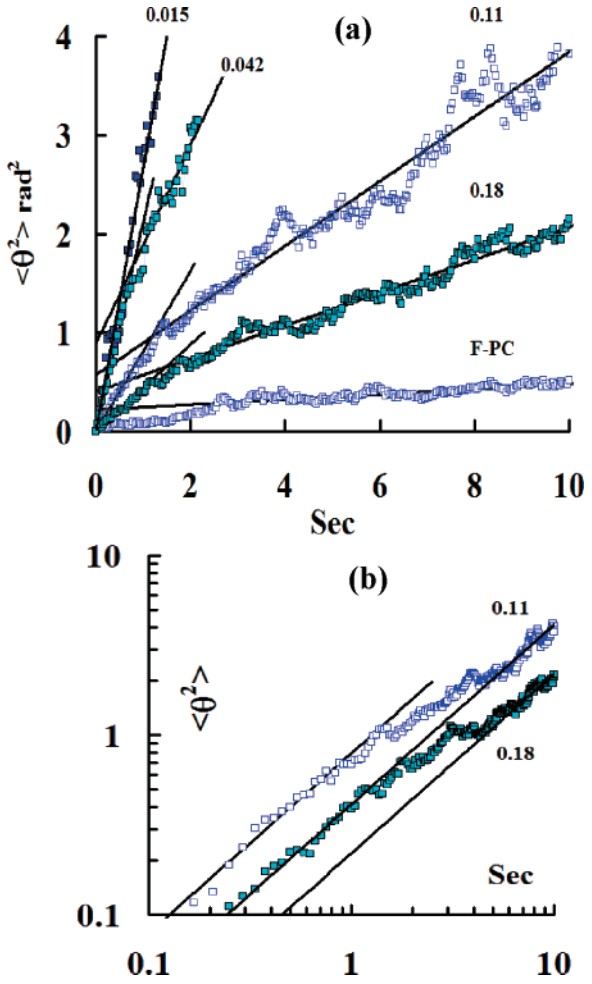

Figure 7. (a) Mean-square rotational displacements, $\langle\theta(t)^2\rangle$, of Se rods for $\phi = 0.015-0.18$, and for the free 4−10 PCs (F-PC) in $\phi = 0.18$, where two straight lines of each curve show its initial and final slopes, respectively. (b) Log−log representation of the curves for $\phi = 0.11$ and 0.18. The respective straight lines have unit slope, and the number of each curve denotes ϕ.

Table 1. Translational and Rotational Diffusion Coefficients, D_T and D_θ, of Se rods for $\phi = 0.015-0.18$, and for the Free 4−10PCs (F-PC) in $\phi = 0.18$, Where the Superscripts, s and 1, for D_T and D_θ, Indicate the Short- and Long-Time Regimes, Respectively

	D_T (μm²/s)		D_θ (rad²/s)	
ϕ	D_T^s	D_T^l	D_θ^s	D_θ^l
0.015	2.41×10^{-1}		1.54	
0.042	1.20×10^{-1}		1.06	5.04×10^{-1}
0.11	3.23×10^{-2}	1.67×10^{-2}	0.448	1.64×10^{-1}
0.18	1.85×10^{-2}	8.30×10^{-3}	0.219	8.34×10^{-2}
F-PC	1.06×10^{-2}	1.99×10^{-3}		1.31×10^{-2}

D_T^l/D_T°, for $\phi = 0.11$ and 0.18 are determined to be 1.69×10^{-2}, and 8.40×10^{-3}, respectively. However, 2D Brownian dynamics computer simulations of Lahtinen et al. have shown that D_T^l/D_T^0 for hard rods with $P = 6$ at surface densities corresponding to $\phi = 0.11$ and 0.18 ($\rho = (H_0/W)\phi$) is about 0.6 and 0.4, respectively.[21] Such a large difference between our values and the simulations may be mainly for two reasons: electrostatic repulsions and hydrodynamic interactions. The Se rod suspensions we prepared have an extremely low ionic concentration of 1×10^{-6} M, where the rods interact with long-range electrostatic repulsions. However, hard-core rods (used in computer simulations) can be approximated by colloidal rods with very short-ranged repulsions, which can be realized in suspensions with high ionic concentrations when the bare width of the rods is much larger than the Debye screening length. In fact, the width of the Se rods is about 230 nm and the Debye length is 3.08 nm for a high ionic concentration of 1×10^{-2} M. Thus, the long-ranged repulsions can be considered to be one reason for the large reduction in D_T^l/D_T^0.

By Brownian dynamics computer simulations, Kirchhoff et al. have shown a reduction of D_T due to repulsions for rods interacting with a Yukawa-type segment−segment interaction.[23] Moreover, with FRAP, Bruggen et al.[29] have found that D_T^l/D_T^0 for boehmite rods in semidilute suspensions is much smaller than that predicted by the 3D computer simulations of Löwen.[19a] On the other hand, with latex spheres, Blaaderen et al. have shown that D_T more dramatically decreases with increasing ϕ as the Debye length increases.[35]

Hydrodynamic interactions may also reduce D_T^l/D_T^0 of rods in dense suspensions. Li et al.[36] have observed that D_T^l and D_θ^l of single F-actin filaments (2−4.5 μm in length) confined in a thin cell (0.7−1.6 μm in thickness) are smaller by a factor of 2 than those in the bulk dilute solution and accounted for such phenomena by introducing hydrodynamic interactions. They also have showed that D_T^l and D_θ^l are decreased greatly as the filaments approach the cell wall and their length decreases. On the other hand, the length of Se rods (0.82 μm) is fairly short and their width (0.24 μm) is much larger than that of the F-actin filaments, respectively, and besides, the face-to-face distances between Se rods for $\phi = 0.11$ and 0.18 are approximately 0.2 μm. Thus, when these values are considered, D_T^l and D_θ^l for the Se rods in dense suspensions must be reduced more by hydrodynamic interactions.

Rotational Diffusion Coefficients. The rotational diffusion coefficient, D_θ, is obtained by using the equation, $D_\theta = \langle\theta(t)^2\rangle/2t$ (for one dimension). Table 1 also shows the short- and long-time rotational diffusion coefficients, D_θ^s and D_θ^l, respectively, estimated for Se rods in $\phi = 0.015-0.18$ and for the F-PC. On the other hand, the rotational diffusion coefficient of noninteracting rods, D_θ^0, is formulated by Tirado et al.[34] as,

$$D_\theta^0 = 3k_BT(\ln P - 0.662 + 0.917/P - 0.05/P^2)/\pi\eta L^3 \qquad (2)$$

By substituting the dimensions of the Se rod into eq 2, D_θ^0 is calculated to be 6.559 (rad)²/s. Using this value, normalized diffusion coefficients, D_θ^l/D_θ^0, of the Se rods for $\phi = 0.042$, 0.11, and 0.18 are calculated to be 7.68×10^{-2}, 2.49×10^{-2}, and 1.27×10^{-2}, respectively. However, with 2D Brownian dynamics computer simulations, Lahtinen et al.[21] have predicted $D^l\theta/D_\theta^0$ for hard rods of $P = 6$ at surface densities corresponding to $\phi = 0.042$, 0.11, and 0.18 to be 0.85, 0.6, and 0.3, respectively. Like D^l_T/D_T^0, such a

Table 2. Translational and Rotational Plateau Values $\langle R^2\rangle^{1/2}$ and $\langle \theta^2\rangle^{1/2}$ at Appearance Time of Plateau, Denoted by R^* and θ^*, Respectively, of Se Rods for $\phi = 0.11$ and 0.18, and for the Free 4−10 PCs (F-PC) and Constrained 4−8 PCs (C-PC)

ϕ	R^* (μm)	θ^* (deg)
0.11	0.285	48.9
0.18	0.188	40.4
F-PC	0.168	33.8
C-PC	0.126	27.5

large discrepancy between our values and the computer simulations may be due to interparticle electrostatic repulsions.

By using an electric birefringence method, Krammer et al. have measured D_θ of fd virus in concentrated solutions and found a drastic reduction in D_θ with decreasing ionic strength of the solutions.[26] By computer simulations, Kirchhoff et al.[23] have calculated D_θ for rods interacting with a Yukawa-type segment−segment interaction, qualitatively explaining the experiments of Krammer et al. In addition, with optical birefringence, Kluijtmans et al. have measured D_θ of silica-boehmite rods in suspensions and found a drastic decrease of D_θ with decreasing ionic concentration of the suspensions.[28]

Estimation of Plateau Values. A caging effect (due to clustering) in $\langle R(t)^2\rangle$ of Se rods becomes remarkable at $\phi \geq 0.11$. Table 2 shows $\langle R^2\rangle^{1/2}$ and $\langle \theta^2\rangle^{1/2}$ at the time that the plateau appears (although this is not strict), i.e., R^* and θ^*, respectively, of Se rods for $\phi = 0.11$, 0.18, and for the free 4−10PCs (F-PC) and constrained 4−8PCs (C-PC) in $\phi = 0.18$ suspensions, where R^* and θ^* decrease with increasing ϕ. The values of R^* can be a measure of the cage sizes. The values of θ^* are not small in spite of high particle concentrations, and this may be characteristic of synchronized rotations of the cluster rods.

Summary. We synthesize monodisperse Se colloidal rods and investigate their dynamics and arrangement in suspensions with an extremely low ionic strength. Dependence of cluster-size distributions and persistence times on ϕ are determined. Some fundamental microscopic motion modes of the individual rods are found. Measured mean-square displacements of the rods suggest a cage effect (due to rod clustering) and two distinct diffusions. Estimated D_T and D_θ of the Se rods suggest a drastic suppression of their diffusive motions in the dense suspensions due to inter-rod repulsions. This direct observation enables relating the microscopic dynamics of the rods with their macroscopic transport coefficients, which is not accessible with ensemble-averaged experiments.

References

(1) Onsager L. *Ann. N. Y. Acad. Sci*. **1949**, *51*, 627.
(2) Stroobants, A.; Lekkerkerker, H. N. W.; Frenkel, D. *Phys. Rev. A* **1987**, *36*, 2929.
(3) Bolhuis, P. G.; Frenkel, D. *J. Chem. Phys.* **1997**, *106*, 666.
(4) Bolhuis, P. G.; Stroobants, A.; Frenkel, D.; Lekkerekerker, H. N. W. *J. Chem. Phys*. **1997**, *107*, 1551.
(5) Kramer, E. M.; Herzfeld, J. *Phys. Rev. E* **2000**, *61*, 6872.
(6) Buining, P. A.; Philipse, A. P.; Lekkerkerker, H. N. W. *Langmuir* **1994**, *10*, 2106.
(7) Maeda, Y.; Hachisu, S. *Colloids Surf.* **1983**, *6*, 1; *7*, 353.
(8) Maeda, H.; Maeda, Y. *Langmuir* **1995**, *12*, 1446.
(9) Maeda, H.; Maeda, Y. *Phys. Rev. Lett.* **2003**, *90*, 18303.
(10) Maeda, H.; Maeda, Y. *J. Chem. Phys*. **2004**, *121*, 12655.
(11) Mohraz, A.; Solomon, M. J. *Langmuir* **2005**, *21*, 5298.
(12) Wen, X.; Meyer, R. B.; Caspar, D. L. D. *Phys. Rev. Lett*. **1989**, *63*, 2760
(13) Dogic, Z.; Fraden, S.; *Phil. Trans. R. Soc. London, Ser. A* **2001**, *359*, 997.
(14) Dogic, Z.; Purdy, K.; Grelet, E.; Adams, M.; Fraden, S. *Phys. Rev. E* **2004**, *69*, 051702.
(15) Doi, M.; Edwards, S. F. *J. Chem. Soc., Faraday. Trans* 2 **1978**, *74*, 560.
(16) Doi, M.; Edwards, S. F. *The Theory of Polymer Dynamics*; Clarendon Press, Oxford, 1986.
(17) Frenkel, D.; Maguire, J. F. *Mol. Phys*. **1983,** *49*, 503.
(18) Fixman, M. *Phys. Rev. Lett.* **1985**, *54*, 337; *55*, 2429.
(19) (a) Löwen, H. *Phys. Rev. E* **1994**, *50*, 1232. (b) Löwen, H. *Phys. Rev. E* **1999**, *59*, 1989.
(20) Cobb, P. D.; Butler, J. E. *J. Chem. Phys*. 2005, *123*, 054908.
(21) Lahtinen, J. M.; Hjelt, T.; Ala-Nissila, T.; Chovj, Z. *Phys. Rev. E* **2001**, *64*, 021204.
(22) Yu-Guo Tao; den Otter, W. K.; Padding, J. T.; Dhont, J. K. G.; Briels, W. J. *J. Chem. Phys.* **2005**, *122*, 244903.
(23) Kirchhoff, Th.; Löwen, H.; Klein, R. *Phys. Rev. E* **1996**, *53*, 5011.
(24) Moreno, A.; Kob, W. *J. Chem. Phys.* **2004**, *121*, 380.
(25) Cush, R.; Dorman, D.; Russo, P. S. *Macromolecules* **2004**, *37*, 9577.
(26) Krammer, H.; Deggelman, M.; Graf, C.; Hagenbüchle, M.; Johner, C.; Weber, R. *Macromolecules* **1992**, *25*, 4325.
(27) van Bruggen, M. P. B.; Lekkerkerker, H. N. W.; Dhont, J. K. G. *Phys. Rev. E* **1997**, *56*, 4394.
(28) Kluijtmans, S. G. J. M.; Koenderink, G. H.; Philipse, A. P. *Phys. Rev. E* **2000**, *61*, 626.
(29) van Bruggen, M. P. B.; Lekkerkerker, H. N. W.; Maret, G.; Dhont, J. K. G. *Phys. Rev. E* **1998**, *58*, 7668.
(30) Lettinga, M. P.; Barry, E.; Dogic, Z. *Europhys. Lett.* **2005**, *71*, 692.
(31) Saxton, M. J.; Jacobson, K. *Annu. Rev. Biophys. Biomol. Struct*. **1997**, *26*, 373.
(32) Megen W. V. *J. Phys.: Condens. Matter* **2002,** *14*, 7699.
(33) Weeks, E. R.; Weitz, D. A. *Phys. Rev. Lett.* **2002**, *89*, 095704-1.
(34) Tirado, M. M.; Martinez, C. L.; de la Torre, J. G. *J. Chem. Phys.* **1984**, *81*, 2047.
(35) van Blaaderen, A.; Peetermans, J.; Maret, G.; Dhont, J. K. G. *J. Chem. Phys.* **1992**, *96*, 4591.
(36) Li, G.; Tang, J. X. *Phys. Rev. E* **2004**, *69*, 061921.

NL071577I